# Evaluations on aero-optic effects of subsonic airborne electro-optical system

**Kexin Yin (殷柯欣) and Huilin Jiang (姜会林)**

*Changchun University of Science and Technology, Changchun 130022*

Received February 24, 2006

A simple method based on CFD code and Matlab for aero-optic effects is presented. Density fluctuation from CFD code due to the changes of such factors as altitude, speed, equipment location, and wavelength is introduced as an input to Matlab. The overall calculations are in Matlab. The results show that the performance of electro-optical (EO) system can be improved when the altitude increasing, the speed is as slowly as possible, and the equipment location moves to the leading edge of the airborne platform as far as possible, for the wavelength there is an optimum one when the indexes of contrast and resolution of the system are both considered. All of these methods can minimize the optical aberrations. Several numerical simulations demonstrate the method.

*OCIS codes:* 010.1330, 010.3310, 000.4430.

When an otherwise-collimated laser beam passes through a turbulent flow with variable index of refraction, its wavefront becomes dynamically aberrated. These aberrations degrade the beam's ability focused on the far field, so reducing the system utility of the beam that may be used for communication. When the laser platform is an aircraft, one of the causes of beam degradation is the thin layer and immediate air flow around the aircraft, which is referred to the aero-optic effects (see Fig. 1). It is necessary to quantitatively evaluate these degradations for correct and reliable airborne electro-optical (EO) system. A wide variety of different methods have been developed for aero-optical measurements. Daniel[1] applied a Shack Hartman wavefront sensor to measure the optical distortions caused by the density fluctuation. Jiang[2] introduced a novel two-dimensional (2D) Hartman wavefront sensor to measure aero-optic effects when the beam passes through a low velocity heat turbulent jet. The wind tunnel tests have been made successfully in American since 1980s' and until recently American and Israel have cooperated to develop an "arrow" missile that solved a series of aero-optical problems and succeeded in the flying test[3]. Jumper *et al.* have demonstrated a small aperture beam technique (SABT) for quantifying the optical wavefront distortions imposed by passing through the turbulent flow field[4]. The studies of aero-optic field in China originated from 1990s' and made great progress, the investigative emphasis has been gradually transferred from the initial understanding of aero-optical statistical characteristics to the mechanism.

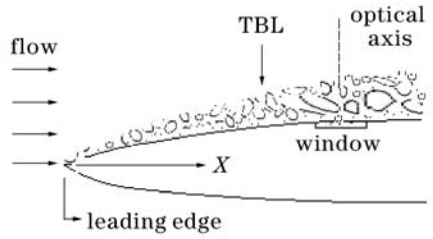


Fig. 1. Schematic of TBL adhere to the airborne platform.

Though some facilities or techniques have been developed to test aero-optical wavefront distortions[5−8], the advances in aero-optical computational simulations have not come as rapidly. The computational simulations play a vital, complementary role in test planning as well as test data interpretation. This paper introduces a simple computational simulation methodology for evaluating aero-optic effects around subsonic airborne EO system based on the combination of CFD code and Matlab. Several numerical simulations that demonstrate the method are presented. The results show that the proposed method can easily assess the aero-optic effects around airborne EO system and make useful predictions or corrections.

Density fluctuation is a key parameter for evaluating aero-optic effects in aerodynamic flow field. In the present study, we use FLUENT[9] to produce density fluctuation. FLUENT is a multiblock CFD code, which can solves the three-dimensional (3D) Navier-Stokes equations. Here flow is turbulent and a regular $k$-$\varepsilon$ model is chosen as current flight conditions. Several parameters such as altitude (affects pressure and density) and Mach number must be specified in FLUENT simulation. Then the turbulent effects are calculated based on turbulent model. The output data of FLUENT code are a discrete set of air density values on an unstructured grid and are resolved in a fluid density file for later use. In this paper we use ICEM CFD 4.1.3 mesh generator that is a multiblock grid generator to produce computational mesh and we make sure that the grid around the window is dense enough. With the comprehensive studies, it has been found that the density fluctuation in turbulent boundary layer (TBL) is determined by the density difference (between wall density and free stream density) that comes from the flow velocity variations due to the increases of the temperature and the fluid speed in the boundary layer. We have an assumption that the density discontinuity occurs in TBL, the peak density is in the middle of overall TBL, and its average value is 10% of this density difference, defined by[10]

$$\rho'_{\text{average}} \cong \rho' \cong |\rho_{\text{w}} - \rho_0| \times 10\%, \tag{1}$$

where $\rho_{\text{w}}$ is wall density and $\rho_0$ is free stream density.

$\rho_{\rm w}$ is easy to access in fluid density file, because the free stream is governed by a number of factors such as altitude, pressure, and temperature that result in the continual changes in weather patterns. Here we adopt international standard atmosphere (ISA) table[11] for $\rho_0$ with different altitudes. FLUENT code is not designed for optical calculations, so for evaluating the density fluctuation we propose a subroutine (function), which calls fluid density file and ISA table for the wall density and free stream density, respectively, and in return is provided with the density fluctuation.

Density fluctuation in TBL leads to variable index of refraction (through Gladstone-Dale "constant") that degrades the performance of airborne EO system such as bore-sight error or intensity reduction on the target. These aberrations to the system can be assessed in a number of ways, however, this reduction is usually quantified in terms of the time-averaged strehl ratio as[12]

$$S \cong \frac{I}{I_0} \cong \exp[-(K\sigma)^2], \tag{2}$$

where $I$ is average on-axis intensity on the target, $I_0$ is ideal or diffraction-limited intensity, and $K = 2\pi/\lambda$ is wave number. $\sigma^2$ is wavefront variance, which depends on two aerodynamic parameters[13] of density fluctuation $\rho'$ and correlative length $l_z$ along the optical axis

$$\sigma^2 = 2G^2 \int_0^{\delta} \langle \rho' \rangle^2 l_z \mathrm{d}z \qquad (l_z \ll \delta), \tag{3}$$

the approximate wavefront deviation is

$$\sigma \approx \sqrt{2 l_z \delta} G \rho', \tag{4}$$

where $G$ is the Gladstone-Dale "constant" strongly depends on gas type, $\delta$ is the boundary layer thickness close to 1.5% of $X$ (the flow distance from the leading edge of airborne platform to the optical platform as shown in Fig. 1), and we assume that $l_z$ is only 10% of $\delta$.

In this section we will discuss the optical aberrations produced by some factors such as flying altitude, speed, equipment location, and wavelength. Density fluctuation can be computed by FLUENT code under different conditions. We assume that the aperture diameter is 30 cm and the relative dispersion angle $\theta_\beta$ is[13]

$$\theta_\beta = \theta_{\rm D}/\sqrt{S}, \tag{5}$$

where $\theta_{\rm D} = 2.4\lambda/D$ is the optical diffraction-limited angle.

Situation 1: the wavelength is 0.5 $\mu$m, the distance $X$ from the leading edge of airborne platform to the optical platform is 10 m, the Mach number is 0.6, and the regularity of the system performance with altitude is shown in Fig. 2. When altitude changes from 1 to 12 km, Strehl increases by 2.5 times, $\sigma$ and $\theta_\beta/\theta_{\rm D}$ decrease by 59% and 46%, respectively. The platform optical system performance improves with altitude increasing because the communication channel can avoid much atmospheric interference, that is to say that the platform attitude is stabilized easily and the system performance can be improved.

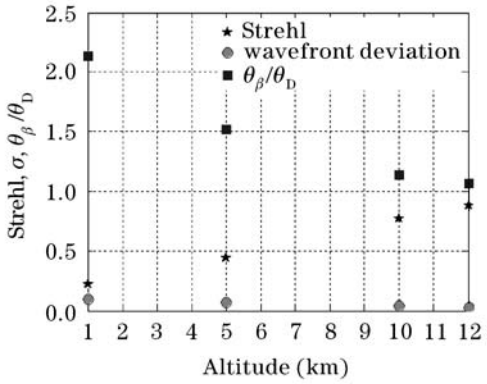


Fig. 2. System performance with altitude.

Situation 2: the conditions are the same as situation 1 except that the Mach number changes from 0.2 to 1. Figure 3 indicates that Mach number has a great effect on the system performance. Strehl decreases by 52% and $\sigma$ increases nearly 20 times when Mach number is from 0.2 to 1. $\theta_\beta/\theta_{\rm D}$ increases by 6% when the Mach number is from 0.2 to 0.6 but increases by 44% when the Mach number is from 0.6 to 1.0. Figure 4 shows the relation between wall density and Mach number, it is clear that at a given altitude of 12 km, with the Mach number increasing the wall density decreases so that both density fluctuation and wavefront deviation increase. In this situation, the speed should be as slowly as possible otherwise it will lead to the great changes of flow density

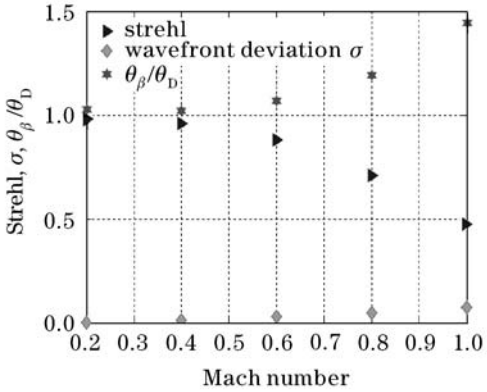


Fig. 3. System performance with Mach number.

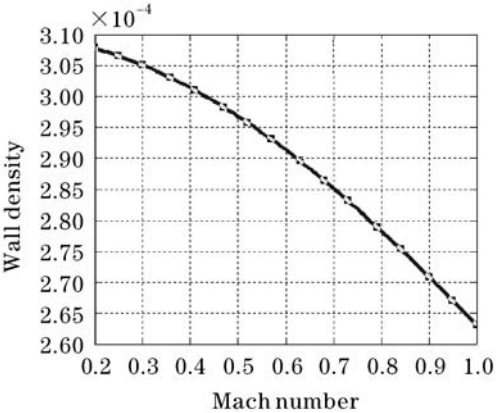


Fig. 4. Wall density with Mach number. Altitude is 12 km.

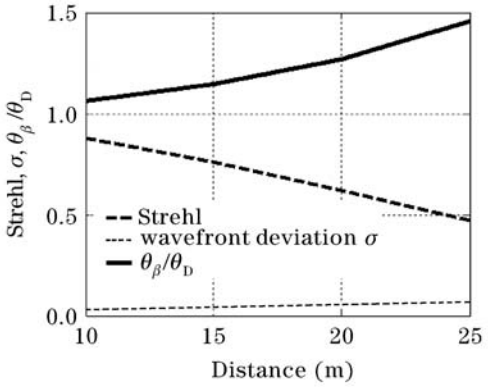


Fig. 5. System performance with distance.

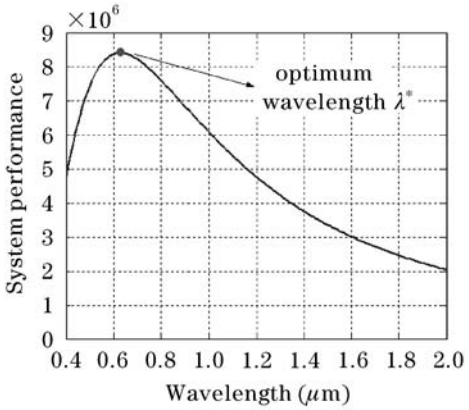


Fig. 7. Optimum wavelength. Altitude is 10 km, $X$ is 25 m, Mach number is 0.6.

and index of refraction because of the variations of flow temperature and velocity.

Situation 3: the initial conditions are the same as situation 1 except that $X$ changes from 10 to 25 m with step 5 m. It is clear that Strehl decreases by 30%, $\sigma$ increases 1.04 times and $\theta_\beta/\theta_\mathrm{D}$ increases by 19% when $X$ is from 10 to 20 m. While Strehl decreases by 47%, $\sigma$ and $\theta_\beta/\theta_\mathrm{D}$ increase by 24% and 37% respectively when $X$ is from 20 to 25 m as shown in Fig. 5. This is because boundary layer begins as a laminar flow with zero thickness at the leading edge of airborne platform (as shown in Fig. 1) or finite thickness on a blunt object. After some distance downstream the laminar flow undergoes transition to turbulent flow. Turbulent is chaotic and seemingly random motion of fluid parcels while fluid parcels of lamina are homogeneous and hardly any fluctuation of index of refraction of the medium that surrounds the system. The transition from lamina to turbulence could occur at Reynolds number as high as $1 \times 10^6$. When lamina turns to turbulence or at the extender of the aerodynamic body, the heterogeneity in the temperature and pressure of the atmosphere leads to variations of the refractive index and density discontinuity. These variations can cause fluctuations in both the intensity and the phase of the received signal. So in this case, the optical window should be moved to the leading edge of the airborne platform as far as possible in order to reduce the optical aberrations.

Situation 4: the altitude is 10 km, $X$ is 25 m, the Mach number is 0.6, and the wavelength changes from 0.4 to 2 $\mu$m. We can see that Strehl increases with wavelength increasing, and when the wavelength is 2 $\mu$m Strehl reaches the local maximum (see Fig. 6). When wavelength is about 0.6 $\mu$m, the dispersion angle $\theta_\beta$ reaches the minimum and that is to say that the resolution of the system is best at this time. Because when the wavelength is increasing, the diffraction limits the performance of the system, and when the wavelength is decreasing, the system aberrations dominate the performance at this time. So we can predict that for a given aero-optic aberration there must be an optimum wavelength that corresponds to the best system performance. For simplifying the problem we have two assumptions: 1) system is diffraction-limited, 2) optical beam jitter is neglected. A new variable $P$ is defined for describing the system performance, which is a ratio between the system indexes of contrast and resolution

$$P = \frac{\exp(-(2\pi\sigma/\lambda)^2)}{(\lambda/D)^2}, \tag{6}$$

where $D$ is the aperture diameter. From

$$\partial P/\partial\lambda = 0, \tag{7}$$

the optimum wavelength $\lambda^*$ is

$$\lambda^* \approx 2\pi\sigma. \tag{8}$$

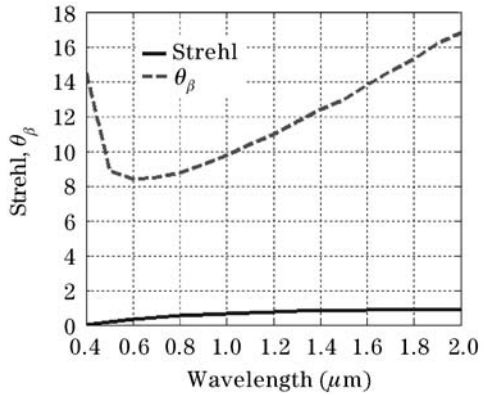


Fig. 6. System performance with wavelength.

Figure 7 shows the system performance with the wavelength. With the wavelength increasing nearly to $\lambda^*$ the system performance increases, but when it is larger than $\lambda^*$ the performance decreases. Though there are some factors that make it difficult to choose the optimal $\lambda^*$ such as the poor transmittance of the optical platform (window) or no suitable detector that has enough sensitivity at $\lambda^*$ and so on. But we can choose a much better one that satisfies the specific requirements to get to the best performance.

This paper presented a simple technique for aero-optic evaluations that is based on the synergetic combination of CFD code and Matlab. We carried out CFD calculations using FLUENT and the flow is $k$-$\varepsilon$ model. The output data of FLUENT is given in the form of a discrete set of air density values on an unstructured grid and saved in a fluid density file. The influences of such factors as flying altitude, speed, equipment location and wavelength lead to the density fluctuation, which is available by accessing a user-defined subroutine and ISA table for

the wall density and free steam density respectively. Having introduced density fluctuation into Matlab, we can easily evaluate the wave front variance, Strehl ratio and dispersion angle $\theta_\beta$. With the proposed method, optical engineers can easily assess the aero-optic effects around the airborne EO system and make useful predictions or corrections with respect to above factors.

This work was supported by the National "863" Program of China. K. Yin's e-mail address is ykx@cust.edu.cn.

## References

1. D. R. Neal, E. Hedlund, M. Lederer, A. Collier, C. Spring, and B. Yanta, in *Proceedings of 20th Advanced Measurement and Ground Testing Technology Conference* AIAA 2701 (1998).
2. Z.-F. Jiang, F.-J. Xi, J. Hou, and W.-Y. Li, Chin. J. Lasers (in Chinese) **31,** 943 (2004).
3. X. Yin, Engineering Science (in Chinese) **7,** 1 (2005).
4. E. J. Jumper and R. J. Hugo, AIAA Journal **33,** 2151 (1995).
5. B. F. Carroll, E. Boulos, M. Systma, L. N. Cattafesta, J. P. Hubner, and M. Sheplak, in *Proceedings of 42nd American Institute of Aeronautics and Astronautics Aerospace Sciences Meeting and Exhibit* AIAA 936 (2004).
6. N. Sinha and S. Arunajatesan, in *Proceedings of 35th American Institute of Aeronautics and Astronautics Plasmadynamics and Lasers Conference* AIAA 2448 (2004).
7. C. Wyckham, S. H. Zaidi, R. B. Miles, and A. Smits, in *Proceedings of 36th American Institute of Aeronautics and Astronautics Plamadynamics and Lasers Conference* AIAA 4775 (2005).
8. S. Gordeyev, D. Duffin, and E. Jumper, in *Proceedings of International Conference on Advanced Optical Diagnostics in Fluids, Solids and Combustion* v0020 (2004).
9. Fluent news, Newsletter Vol. **10**, Issue 2, winter 2001, Lebanon, N.H 03766 USA.
10. E. Tromeur, E. Garnier, and P. Sagaul, J. Fluids Eng. **128,** 239 (2006).
11. http://selair.selkirk.bc.ca/aerodynamics1/Appendix/ISA_Table.html.
12. X.-W. Du, Chin. J. Lasers (in Chinese) **24,** 327 (1997).
13. N. E. Dalrymple, *Mirror seeing, Advanced Technology Solar Telescope* Project Document, PRT-0003 (REV A) (2002).